

Chemically stable polyarylether-based covalent organic frameworks

Xinyu Guan, Hui Li, Yunchao Ma, Ming Xue, Qianrong Fang, Yushan Yan, Valentin Valtchev, Shilun Qiu

▶ **To cite this version:**

Xinyu Guan, Hui Li, Yunchao Ma, Ming Xue, Qianrong Fang, et al.. Chemically stable polyarylether-based covalent organic frameworks. Nature Chemistry, 2019, 11 (6), pp.587-594. 10.1038/s41557-019-0238-5 . hal-03035133

HAL Id: hal-03035133

https://normandie-univ.hal.science/hal-03035133

Submitted on 2 Dec 2020

HAL is a multi-disciplinary open access archive for the deposit and dissemination of scientific research documents, whether they are published or not. The documents may come from teaching and research institutions in France or abroad, or from public or private research centers.

L'archive ouverte pluridisciplinaire **HAL**, est destinée au dépôt et à la diffusion de documents scientifiques de niveau recherche, publiés ou non, émanant des établissements d'enseignement et de recherche français ou étrangers, des laboratoires publics ou privés.

Chemically stable polyarylether covalent organic frameworks

Xinyu Guan,[1] Hui Li,[1] Yunchao Ma,[1] Ming Xue,[1] Qianrong Fang,[1*] Yushan Yan,[2*] Valentin Valtchev[1,3*] and Shilun Qiu[1]

[1]*State Key Laboratory of Inorganic Synthesis and Preparative Chemistry, Jilin University, Changchun 130012, China*

E-mail: qrfang@jlu.edu.cn

[2]*Department of Chemical and Biomolecular Engineering, Center for Catalytic Science and Technology, University of Delaware, Newark, DE 19716, USA*

E-mail: yanys@udel.edu

[3]*Normandie Univ, ENSICAEN, UNICAEN, CNRS, Laboratoire Catalyse et Spectrochimie, 6 Marechal Juin, 14050 Caen, France*

E-mail: valentin.valtchev@ensicaen.fr

Abstract

The development of crystalline porous materials (CPMs) with high chemical stability is of paramount importance for their practical uses. Here we report the synthesis of novel polyarylether covalent organic frameworks (PAE-COFs) with high crystallinity, porosity and exceptional chemical stability due to the inert nature of polyarylether building blocks. We demonstrate that these materials can be stable against harsh chemical environments involving boiling water, strong acids/bases, oxidation and reduction conditions, which exceed all known CPMs, including zeolites, metal-organic frameworks (MOFs) and COFs. Furthermore, we explore their advantages as an efficient platform for structural design and functional evolution. The functionalized PAE-COFs combine porosity, high stability, and recyclability, and deliver outstanding performance in the removal of antibiotics from water over a wide pH range.

Introduction

Covalent organic frameworks (COFs) are an emerging class of crystalline porous materials (CPMs), which are composed of organic building blocks linked by strong covalent bonds.[1-6] Over the past decade, COFs have attracted wide attention in various application fields including gas adsorption and separation,[7-9] catalysis,[10-13] electrochemistry,[14-16] and a number of others.[17-22] Nonetheless, the linkages of available COFs are limited to B-O, C=N, C-N, C=C and B=N bonds. Furthermore, low chemical stabilities, especially in acid and base, present a considerable hindrance to the further development and application of COFs. Although structural stabilities of some COFs can be improved by hydrogen bonds,[23] keto-enol tautomerism,[24] enhanced interlayer interactions[25] or conversion of the imine linkages,[26] these materials do not survive harsh chemical environments, e.g., enhanced acid/base concentration. Design and preparation of a new class of robust COFs that are stable under extreme conditions thus remains a major challenge for bringing these exceptional materials to practical applications.

Polyarylether (PAE) is a highly stable engineered plastic with high heat resistance, excellent chemical stability, good flame retardant properties, and high mechanical robustness.[27] PAEs can be easily modified with various functional groups[28] including cyano, carbonyl, carboxyl, and sulfo groups, and thus have broad application prospects in the aerospace, rail transportation, automobile manufacturing, machinery industry and many other technological fields.[29] Polymers of intrinsic microporosity (PIMs), a new kind of porous material connected by ether bonds, have recently been reported.[30] However, PIMs are amorphous phases without uniform and ordered pores, which limits their potential applications. The synthesis of crystalline porous PAEs will grant this material with all the advantages of crystalline porous solids, such as a defined channel system that is able to perform recognition and separation of close in size molecules, and an extended micro- and/or mesoporous volume and functional surface with crystallographically defined positions.

Herein, we address the above issues by synthesizing a new kind of polyarylether-based covalent organic frameworks (PAE-COFs) that combine high crystallinity, porosity, and outstanding stability. Two novel PAE-COFs with micropores of 16.8 Å and mesopores of 28.4 Å, denoted as JUC-505 and JUC-506 (JUC = Jilin University China), were successfully synthesized. JUC-505 features excellent carbon dioxide (CO_2) adsorption (231.3 mg g^{-1} at 273 K and 189.0 mg g^{-1} at 298 K) and separation

(48.9 for CO_2/CH_4 and 97.2 for CO_2/N_2), which are among the highest reported for COF and PIM materials. Remarkably, PAE-COFs maintain their crystallinity after the treatment under harsh chemical environments, including boiling water, strong acids (HCl, H_2SO_4 and HF) and bases (NaOH and MeONa), oxidation (chromic acid lotion) and reduction ($LiAlH_4$) medium, which outstrips all known CPMs including the aluminosilicate zeolites, metal-organic frameworks (MOFs) and COFs. These COFs with high stability, crystallinity and porosity provide a material platform for structural design and functional development. PAE-COFs with carboxyl or amino functional groups, denoted JUC-505-COOH and JUC-505-NH_2, were subsequently obtained by the post-synthetic functionalization, and showed a remarkable performance in the removal of antibiotics from water over a wide pH range (pH = 1-13).

Results and discussion

Design of PAE-COFs. Our strategy for preparing PAE-COFs involves aromatic nucleophilic substitution between the extended *o*-difluoro benzene and catechol building units catalyzed by anhydrous potassium carbonate. In the model condensation reaction of tetrafluoroterephthalonitrile (TFTPN) with 1,2-dihydroxybenzene (DHB), fluoride ion and proton are eliminated to yield a dioxin product, 3,13-dicyanobenzo-1,2,4',5'-bis(1,4-benzodioxane) (DCBD, Fig. 1a). On the basis of this reaction, DHB is extended to a triangular building unit, 2,3,6,7,10,11-hexahydroxytriphenylene hydrate (HHTP), whereas TFTPN can be employed directly or replaced by other linear building blocks, such as 2,3,6,7-tetrafluoroanthraquinone (TFAQ). As shown in Fig. 1b, the condensation reaction of HHTP and TFTPN produces a two-dimensional (2D) microporous crystalline JUC-505 with hexagonal pores of 16.8 Å. On the other hand, replacing TFTPN with a longer linker, TFAQ, gives 2D mesoporous JUC-506 with larger hexagonal pores of 28.4 Å (Fig. 1c). By linking the linear and triangular building units through the aromatic nucleophilic substitution reaction, the products form 2D structures based on the boron nitride net (**bnn**, Fig. 1d).

Synthesis and characterization. Typically, PAE-COFs were synthesized by suspending anhydrous potassium carbonate, HHTP with TFTPN or TFAQ in a mixed solution of *N*-methyl-2-pyrrolidone (NMP) and mesitylene followed by heating at 120 °C and 160 °C for 3 days, giving crystalline solids at yields of 84% for JUC-505 and 78% for JUC-506, respectively. Scanning electron microscopy (SEM) inspection revealed that both materials exhibit fiber-like particles with a cross section diameter of about

100 nm. The length of fiber-like particles is several hundred nanometers in the case of JUC-505, while up to 10 micron fibers can be seen in the case of JUC-506 (Figs. S1 and S2). Fourier transform infrared (FTIR) spectra displayed adsorption peaks at 1264 cm^{-1} and 1021 cm^{-1} for JUC-505 and 1270 cm^{-1} and 1031 cm^{-1} for JUC-506 corresponding to asymmetric and symmetric vibration modes of the ether bonds, respectively, which is consistent with those from the model compound DCBD (1274 cm^{-1} and 1030 cm^{-1}, Figs. S5-7). Noteworthy, the significant decrease at 3432 cm^{-1} (referring to OH stretching of the starting material HHTP) was observed, indicating a high-conversion polymerization. Solid-state ^{13}C cross polarization magic-angle-spinning (CP/MAS) nuclear magnetic resonance (NMR) analysis resulted in the exact attribution for each peak and further confirmed the formation of PAE-COFs (Figs. S9 and S10). Elemental analysis of PAE-COFs was in good agreement with the expected formulas of $C_{10}H_2O_2N$ for JUC-505 and $C_{13}H_4O_3$ for JUC-506, respectively. The content of residue fluorine was further determined by energy dispersive spectrometer (EDS) as 0.94% for JUC-505 and 0.49% for JUC-506 (Figs. S13 and S15). Furthermore, the reaction conversions were calculated from residue fluorine content as 95.3% for PAE-505 and 96.9% for PAE-506.

Crystallinity and structural resolution. The crystallinity and unit cell parameters of PAE-COFs were determined by powder X-ray diffraction (PXRD) analysis. Data obtained with the Materials Studio software package based on of the eclipsed 2D **bnn** net show that both PAE-COFs crystallize in *P*6/mmm (No. 197) space group (Figs. S17, S20, Tables S1 and S3).[31] After a geometrical energy minimization using the universal force field, the unit cell parameters were obtained ($a = b$ = 24.6865 Å, c = 3.5002 Å, $\alpha = \beta$ = 90° and γ =120° for JUC-505; $a = b$ = 33.7458 Å, c = 3.4702 Å, $\alpha = \beta$ = 90° and γ =120° for JUC-506). The simulated PXRD patterns were in good agreement with the experimental ones (Fig. 2, a and b). Furthermore, full profile pattern matching (Pawley) refinements were carried out on the experimental PXRD patterns. Peaks at 2θ = 4.12, 7.13, 8.24, 10.93 and 14.88° for JUC-505 and 3.02, 5.23, 6.04, 8.00 and 10.91° for JUC-506 correspond to the (100), (110), (200), (210) and (310) planes, respectively. The refinement results yielded unit cell parameters nearly equivalent to the predictions with good agreement factors ($a = b$ = 24.7714 Å, c = 3.4624 Å, $\alpha = \beta$ = 90°, γ =120°, ωRp = 2.02% and Rp = 1.60% for JUC-505; $a = b$ = 33.9363 Å, c = 3.5704 Å, $\alpha = \beta$ = 90°, γ =120°, ωRp = 5.71% and Rp = 3.07% for JUC-506). We also considered an alternative staggered 2D arrangement (AB stacking) in which the units of adjacent sheets are horizontally offset by a distance of a/2 and b/2 (Figs. S18, S21, Tables S2 and S4). The simulated PXRD pattern for this arrangement does not match

the experimental data (Figs. S19 and S22). On the basis of these results, JUC-505 and JUC-506 were proposed to have the eclipsed stacking architectures with hexagonal micropores of about 16.8 Å and hexagonal mesopores of 28.4 Å, respectively (Fig. 2, c and d). The formation of the eclipsed structure can be attributed to the strong tendency for aromatic units to form cofacial aggregates between adjacent layers.

Gas adsorption and separation. Nitrogen (N_2) adsorption-desorption analysis of JUC-505 measured at 77 K showed a type I isotherm with a sharp uptake at a low pressure of $P/P_0 < 0.05$, which is characteristic of microporous material (Fig. 3a). Meanwhile, N_2 adsorption-desorption isotherm of JUC-506 showed a rapid uptake at a low pressure of $P/P_0 < 0.1$, followed by a sharp step between $P/P_0 = 0.15$ and 0.25 (Fig. 3b). This sorption profile is best described as a type IV isotherm, which is characteristic of mesoporous materials. The total pore volumes were evaluated at $P/P_0 = 0.95$ to be Vp = 0.51 $cm^3\ g^{-1}$ for JUC-505 and 0.71 $cm^3\ g^{-1}$ for JUC-506. Pore size distributions of PAE-COFs calculated on the basis of nonlocal density functional theory (NLDFT) showed pore with sizes of 16.2 Å for JUC-505 and 30.1 Å for JUC-506, respectively (Fig. 3 a and b, inset), which is in good agreement with that of the proposed model (16.8 Å for JUC-505 and 28.4 Å for JUC-506). The Brunauer-Emmett-Teller (BET) equation was applied over the $0.02 < P/P_0 < 0.20$ range of the isotherms, revealing BET surface areas of 1584 $m^2\ g^{-1}$ for JUC-505 and 1655 $m^2\ g^{-1}$ for JUC-506 (Figs. S28 and S29).

Considering the high crystallinity, excellent porosity and affinity to CO_2 of PIMs,[30] we studied the potential application of PAE-COFs for CO_2 adsorption and separation. The adsorption isotherms of CO_2, N_2, and CH_4 were measured at 273 K and 298 K, respectively. As shown in Figs. 3, S32 and S33, the sorption amounts of CO_2 are as high as 231.3 mg g^{-1} for JUC-505 and 203.0 mg g^{-1} for JUC-506 at 273 K, and the CO_2 sorption analysis at 298 K shows the capacity of 189.0 mg g^{-1} for JUC-505 and 159.2 mg g^{-1} for JUC-506. Thus, JUC-505 exhibits the highest CO_2 uptake among COFs and PIMs reported to date, such as PyTTA-BFBIm-iCOF (177 mg/g at 273 K)[32] and TZPIMs (132 mg/g at 273 K).[33] Meanwhile, the CO_2 uptake is much higher with respect to other gases such as CH_4 (19.2 mg g^{-1} for JUC-505 and 18.3 mg g^{-1} for JUC-506 at 273 K; 15.2 mg g^{-1} for JUC-505 and 13.1 mg g^{-1} for JUC-506 at 298 K) and N_2 (10.4 mg g^{-1} for JUC-505 and 8.8 mg g^{-1} for JUC-506 at 273 K; 12.5 mg g^{-1} for JUC-505 and 8.9 mg g^{-1} for JUC-506 at 298 K). The ideal adsorption selectivity of PAE-COFs was calculated from the ratio of the initial slopes in the Henry region of the isotherms (Figs. S34–S37),[34]

and high selectivity of CO_2/N_2 and CO_2/CH_4 was observed (Table 1). For example, the ideal adsorption selectivity of JUC-505 is as high as 48.9 for CO_2/CH_4 and 97.2 for CO_2/N_2 at 273 K, respectively. Furthermore, preliminary breakthrough experiments for JUC-505 were carried out by exposing to streams containing binary mixtures of CO_2/N_2 or CO_2/CH_4 (50:50 v/v) at room temperature. The results clearly showed that in both cases only CO_2 was retained in the pores of JUC-505 while N_2 and CH_4 passed through without impediment (Fig. 3 e and f).

Stability of PAE-COFs. Similar to amorphous PAEs, crystalline PAE-COFs displays outstanding thermal and chemical stability. According to the thermogravimetric analysis (TGA), PAE-COFs are thermally stable up to 400 °C under nitrogen (Figs. S38 and S39). To investigate the chemical stability of PAE-COFs, we exposed JUC-505 and JUC-506 samples to different chemical environments for one week, including various organic solvents (e.g., NMP, *N*,*N*-dimethylformamide (DMF), tetrahydrofuran (THF), dichloromethane (DCM), ethanol (EtOH), acetone, n-hexane and *m*-cresol), boiling water, concentrated HCl (12 M), concentrated H_2SO_4 (18 M), HF (40%), concentrated NaOH (14 M), MeONa (5 M in MeOH), chromic acid lotion (0.1 M $K_2Cr_2O_7$ in concentrate H_2SO_4) and $LiAlH_4$ (2.4 M in THF). JUC-505 and JUC-506 retain their original skeleton and crystalline structure after the treatment under the above conditions as demonstrated by unaltered position and strength of the peaks in their PXRD patterns (Figs. 2e and S42) and the retained ether bond in the IR spectra (Figs. 2f and S45). Moreover, N_2 adsorption isotherms at 77 K after the treatment are very close to those of as-synthesized materials, which further confirmed the preserved porosity (Figs. S46 and S47). For the sake of comparison, we tested the chemical stability of the typically stable COFs reported to date, including DhaTab-COF,[23] TpPa-1,[24] TPB-DMTP-COF[25], LZU-190[26], PI-COF-2[35], CS-COF[36] and TpOMe-Pa1[37] (Figs. S48-S54). On the basis of the PXRD analysis, TpPa-1, PI-COF-2, LZU-190, CS-COF, TpOMe-Pa1 and DhaTab-COF are not stable in extreme alkaline medium whereas TPB-DMTP-COF, PI-COF-2 and DhaTab-COF cannot withstand strong acid. Noteworthy, none of these most stable COFs retains crystallinity after the treatment with concentrate H_2SO_4 or chromic acid lotion. Furthermore, some typical MOFs (e.g., UiO-66[38], ZIF-8[39], HKUST-1[40] and MOF-5[41]) and zeolites (commercial Silicalite-1, X, Y and 4A) were also selected for the stability test, and none of these matters retained entire crystallinity after the treatment as can be seen in Table 2 and Figs. S55-S62. These results unambiguously prove the outstanding chemical stability of PAE-COFs which surpasses all known crystalline porous materials.

Functionalization of PAE-COFs. In order to extend the possible applications, JUC-505 was transformed into an open framework with functional sites by the chemical modification of cyano groups (Figs. 1b, S20, S21, Tables S5 and S6). Carboxyl or amino functionalized PAE-COFs, JUC-505-COOH and JUC-505-NH_2, were obtained by refluxing JUC-505 in NaOH (20% in ethanol/water = 1/1)[42] and $LiAlH_4$ (2.4 M in THF),[43] respectively. SEM images of functionalized JUC-505 derivatives exhibited similar morphology to the parent material (Figs. S3 and S4). Adsorption peaks of IR spectra at 1268 cm^{-1} and 1021 cm^{-1} for JUC-505-COOH as well as 1264 cm^{-1} and 1022 cm^{-1} for JUC-505-NH_2, corresponding to asymmetric and symmetric vibration modes of the ether bonds, were consistent with those of the pristine structure (1264 cm^{-1} and 1021 cm^{-1} for JUC-505, Fig. S8). Peaks at 1716 cm^{-1} for JUC-505-COOH and 3293 cm^{-1} for JUC-505-NH_2 indicated the grafting of carboxyl and amino group on the respective COFs. A significant decrease of the peak at 2239 cm^{-1} demonstrated the high transformation ratios of cyano groups for both post-modifications. Furthermore, the peaks at 163 ppm for JUC-505-COOH and 25 ppm for JUC-505-NH_2 from the solid-state ^{13}C CP/MAS NMR analysis confirmed the presence of carboxyl and aminomethyl groups, respectively (Figs. S11 and S12). The PXRD patterns of JUC-505-COOH and JUC-505-NH_2 were identical to JUC-505 (Fig. S23), which showed that the framework was not affected by the grafting. Conversation rates were further determined by CHN elemental analysis as 98.6% for JUC-505-COOH and 94.6% for JUC-505-NH_2. The porosities of JUC-505-COOH and JUC-505-NH_2 were evaluated by N_2-sorption isotherm measurements. Both matters showed typical type I isotherms (Figs. S26 and S27), and the BET surface areas were reduced slightly with respect to the parent material (1392 $m^2\ g^{-1}$ for JUC-505-COOH and 1244 $m^2\ g^{-1}$ for JUC-505-NH_2, Figs. S30 and S31).

Adsorptive removal of antibiotics. Antibiotics, as one of the major classes of pharmaceuticals and personal care products, are widely used in hospitals, households, and veterinary applications, and their production and usage increase every year.[44] However, when released into the environment, they can promote the development of resistance in microbial populations and induce toxic effects on aquatic organisms.[45] Tetracycline antibiotics (TCA) are among the most widely used ones. As an experimental proof-of-concept, three common species of TCA including tetracycline (TC), oxytetracycline (OTC) and chlortetracycline hydrochloride (CTC) were chosen for the adsorption test. The parent JUC-505 and functionalized PAE-COFs (JUC-505-COOH and JUC-505-NH_2) were activated to remove guest molecules and then immersed in antibiotic solutions at pH = 1-13 for 3 days. The residual

concentrations and the medical uptake were determined by UV-Vis spectroscopy and calculated according to the standard curve.

As shown in Fig. 4 a-c, carboxyl-decorated JUC-505-COOH reveals a larger uptake capacity in acidic solutions (e.g., 245.8 mg/g for TC, 213.8 mg/g for OTC and 238.9 mg/g for CTC at pH = 1) while amino-functionalized JUC-505-NH_2 shows better performance under strongly alkaline conditions (e.g., 247.3 mg/g for TC, 237.0 mg/g for OTC and 274.6 mg/g for CTC at pH = 13), which can be attributed to the hydrogen bond and electrostatic interactions at different pHs. These values prove high adsorbing capacities under extreme pH values, which is superior to the best performance materials reported for antibiotic assimilation, such as resins, clays, carbon nanotubes, zeolites, and MOFs.[46-49] We also tested the reusability of PAE-COFs after antibiotics removal. After being immersed in concentrated HCl for 1 h, filtered and washed with water, PAE-COFs were reused for the antibiotics removal. The sorption and release process was repeated for five continuous cycles, and the procedure was reversible with almost no loss of capacity (Fig. 4 d-i). These results suggest that the extremely stable PAE-COFs with high adsorption capacities are excellent materials for antibiotics removal that can be used under extreme conditions, regardless of the pH value.

Conclusion

In summary, we have developed a novel series of crystalline, porous and highly stable COF materials, PAE-COFs, by regulating the crystallization of ultra-highly stable polyarylether. PAE-COFs are thermally stable up to 400 °C and extremely resistant to various chemical environments, including boiling water, strong acids and bases, oxidation and reduction atmosphere, which surpasses all known crystalline porous materials including zeolites, MOFs and COFs. PAE-COFs showed impressive CO_2 adsorption capacity and CO_2/CH_4 and CO_2/N_2 selectivities. A member of the family (JUC-505) recorded the highest CO_2 uptake (231.3 mg g^{-1} at 273 K) overpassing all COFs and PIMs reported to date. Carboxyl or amino functionalized PAE-COFs showed exceptional abilities for antibiotics removal from water covering the pH range of 1-13. These stable novel COFs are a perfect platform for the preparation of functional materials that can be used under extreme chemical environments. Finally, this study shows that the most significantdisadvantage of COF materials, their limited chemical stability, can be overcome by proper design of their skeletons based on new stable bonds.

Methods

Synthesis of TFAQ.[50] A mixture of 4,5-difluorophthalic anhydride (5.0 g, 27.2 mmol) and 1,2-difluorobenzene (16.0 mL, 165.0 mmol) was heated to 60 ºC and stirred for 20 mins. After cooling to room temperature (RT), $AlCl_3$ (7.9 g, 54.0 mmol) was carefully added to the mixture in small portions. The resultant dark brown solution was stirred at RT for 4 hrs, and then the reaction mixture was cooled to 0 ºC and 1 M HCl was slowly added. The white precipitate obtained from the reaction was dissolved in Et_2O, and the organic phase was washed with 1 M HCl and water and dried over Na_2SO_4, and then concentrated under vacuum. Recrystallized from CH_2Cl_2/hexane gave pure TFAQ as a pale-brown solid (7.4 g, 91%) (Rf = 0.35 with $CHCl_3$/MeOH 10:1); m.p. 123 °C; ^{1}H NMR (600 MHz, $CDCl_3$): d = 7.96 (t, J = 9.0 Hz, 1H), 7.63 (t, J = 8.4 Hz, 1H), 7.41 (br s, 1H), 7.23–7.19 ppm (m, 2H); IR (KBr): 3072–2581, 1685, 1611, 1590, 1519, 1435, 1321, 1285, 1180, 904 cm^{-1}.

Synthesis of the model DCBD compound. The model compound, 3,13-dicyanobenzo-1,2,4',5'-bis(1, 4-benzodioxane) (DCBD), was prepared as described previously in the thioamide PIM-1 paper.[51] Anhydrous DMF (60.0 mL) was added to 1,2-dihydroxybenzene (2.2 g, 20.4 mmol), tetrafluoroterephthalonitrile (1.9 g, 9.3 mmol), and potassium carbonate (8.0 g, 57.8 mmol) under an inert atmosphere. The reaction was heated to 65 °C and kept at this temperature for 24 hrs. The mixture was cooled to RT, and the solid was collected via vacuum filtration. The crude product was then stirred in water (150.0 mL) for 1 hr and acetone (150.0 mL) for 1 hr before being dried in an oven at 110 °C overnight. DCBD was obtained as a yellow solid (2.9 g, 90% yield). ^{1}H NMR (400 MHz, DMSO-*d6*) δ: 7.25−7.00 ppm (m, 8H). IR (KBr): 2240, 1607, 1498, 1446, 1099, 1029 cm^{-1}.

Synthesis of JUC-505. A Pyrex tube measuring o.d. × i.d. = 10 × 8 mm^2 was charged with anhydrous K_2CO_3 (138.2 mg, 1.0 mmol), HHTP (32.4 mg, 0.1 mmol) and TFTPN (30.0 mg, 0.15 mmol) in a solution of 0.30 mL mesitylene/0.60 mL NMP. The tube was flash frozen at 77 K (LN_2 bath), evacuated to an internal pressure of 0.15 mmHg and flame sealed. Upon sealing the length of the tube was reduced to ca. 13.0 cm. The reaction mixture was heated at 120 °C for 3 days and the obtained brown precipitate was isolated by filtration over a medium glass frit and washed with DMF (20.0 mL × 3), H_2O (20.0 mL × 3) and acetone (20.0 mL × 3). The solvent was then exchanged with anhydrous acetone and removed under vacuum at 80 °C to afford JUC-505 as a brown powder (42.1 mg, 84%). The degree of crystallinity was calculated from PXRD pattern by Jade[52] as 91.9%. Solid-state ^{13}C NMR (500 MHz) d: 145.5, 137.8, 125.5, 109.7, 93.4. IR (KBr): 3077, 3028, 2239, 1681, 1624, 1506, 1460,

1264, 1185, 1021, 982, 877 cm^{-1}. Anal. Calcd: C, 71.44; H, 1.20; N, 8.33. Found: C, 70.76; H, 1.17; N, 8.14; F, 0.95.

Synthesis of JUC-506. In a manner similar to the preparation of JUC-505, treatment of K_2CO_3 (138.2 mg, 1.0 mmol), HHTP (32.4 mg, 0.1 mmol) and TFAQ (42.0 mg, 0.15 mmol) in a solution of 0.30 mL mesitylene/0.60 mL NMP at 160 °C for 3 days yielded a brown precipitate (48.7 mg, 78%), which was subjected to purification by the above described procedure. The degree of crystallinity was calculated from PXRD pattern by Jade as 85.1%. Solid-state ^{13}C NMR (500 MHz) d: 177.4, 144.9, 138.9, 129.1, 125.0, 113.8, 109.2. IR (KBr): 3071, 1676, 1578, 1519, 1493, 1270, 1179, 1041, 982, 864 cm^{-1}. Anal. Calcd: C, 75.01; H, 1.94. Found: C, 74.64; H, 1.92; F, 0.49.

Synthesis of JUC-505-COOH. JUC-505 powder (200.0 mg) and 20% NaOH solution (H_2O/ethanol = 1/1, 50.0 mL) were added to a one neck round-bottom flask equipped with a condenser. The mixture was heated to 120 °C and left to stir at this temperature under reflux for three days. Samples were filtrated and refluxed in water and 1 M HCl for 2 hrs, respectively. The solid was collected by vacuum filtration, then washed with water and THF. The product was then subjected to Soxhlet extraction with THF as the solvent for one day to remove the trapped guest molecules. The solvent was then exchanged with anhydrous acetone and removed under vacuum at 80 °C giving JUC-505-COOH as a brown powder (211.2 mg, 95%). The degree of crystallinity was calculated from PXRD pattern by Jade as 90.3%. Solid-state ^{13}C NMR (500 MHz) d: 163.2, 143.8, 137.8, 124.7, 108.6. IR (KBr): 3178, 3063, 2987, 2237, 1717, 1682, 1596, 1517, 1682, 1596, 1518, 1428, 1268,1190, 1021, 978, 921, 866 cm^{-1}. Anal. Calcd: C, 64.18; H, 1.62. Found: C, 63.70; H, 1.59.

Synthesis of JUC-505-NH_2. JUC-505 powder (200.0 mg) and $LiAlH_4$ (2.4 M in THF, 30.0 mL) were added to a one neck round-bottom flask equipped with a condenser. The mixture was heated to 90 °C and left to stir at this temperature under reflux for one day. After cooling down to room temperature, 1.0 mL 10% NaOH was added dropwise to quench the reaction. 10.0 mL HCl (HCl/H_2O = 2/1) was then added to the solution and stirred for 1 hr. The solid was collected by vacuum filtration, then washed with water. The residue powder was immersed in 20.0 mL 10% NaOH to remove the extra acid and then exchanged with water until the solution became neutral. The solid was collected by vacuum filtration and washed with water and THF. The product was subjected to Soxhlet extraction with THF as the solvent for one day to remove the trapped guest molecules. The solvent was then exchanged with anhydrous acetone and removed under vacuum at 80 °C giving JUC-505-NH_2 as a brown powder

(188.7 mg, 92%). The degree of crystallinity was calculated from PXRD pattern by Jade as 88.2%. Solid-state ^{13}C NMR (500 MHz) d: 145.5, 138.7, 125.0, 109.1, 25.0. IR (KBr): 3300, 3078, 2941, 2237, 1634, 1587, 1515, 1264, 1186, 1144, 1022, 977, 867 cm^{-1}. Anal. Calcd: C, 69.77; H, 3.51; N, 8.14. Found: C, 69.33; H, 3.38; N, 7.94.

Stability tests. The as-synthesized samples (10.0 mg) were kept for 7 days in 20.0 mL of NMP, DMF, THF, DCM, EtOH, acetone, n-hexane, *m*-cresol, boiling water, HCl (12 M), H_2SO_4 (18 M), HF (40%), NaOH (14 M), MeONa (5 M in MeOH), chromic acid lotion (0.1 M $K_2Cr_2O_7$ in concentrate H_2SO_4) and $LiAlH_4$ (2.4 M in THF). The samples were washed with HCl (HCl/H_2O = 2/1, for samples treated in $LiAlH_4$), water (for samples treated in aqueous solutions), MeOH (for samples treated in MeONa) and THF (for samples treated in organic solvents) respectively, followed by solvent exchanged by acetone and dried under vacuum at 85 °C for 12 hrs and subjected to PXRD, IR and N_2 adsorption analyses.

Sample activation. Before gas-/liquid-phase adsorption experiments, as-synthesized PAE-COFs (50.0 mg) were subjected to Soxhlet extraction with H_2O and acetone as the solvents for one day to exchange the trapped guest molecules. Subsequently, it was collected by filtration and activated by drying under vacuum at 100 °C for 24 hrs.

Antibiotic uptake measurement. At room temperature, activated PAE-COFs (10.0 mg) was transferred to aqueous solutions (20.0 mL) containing given concentrations of TC, OTC or CTC (200.0 mg/L) at each pH value between 1 to 13. After 3 days of soaking (for equilibrium adsorption), the solutions were filtrated and diluted to suitable concentration (among the linearity range of standard curves), and UV-Vis spectrophotometry of the solutions was performed to characterize the adsorption performances of PAE-COFs under specific conditions (360 nm for TC; 268 nm for OTC; 267 nm for CTC). The adsorbed amount Qe for antibiotics was calculated by using the mass balance Equation: $Qe = (C_0\text{-}Ce)V/M$, where C_0 and Ce are the initial and equilibrium concentrations of solutions of antibiotics [mg L^{-1}], V is the volume of solution [L], and M the mass of adsorbent [g].

Characterization. ^1H NMR spectra were recorded on an AV400 NMR spectrometer. ^{13}C CP/MAS NMR spectra were recorded on an AVIII 500 MHz solid-state NMR spectrometer. The FTIR spectra (KBr) were obtained using a SHIMADZU IRAffinity-1 Fourier transform infrared spectrophotometer. A SHIMADZU UV-2450 spectrophotometer was used for all absorbance measurements. TGA was

carried out under nitrogen on a SHIMADZU DTG-60 thermal analyzer at a heating rate of 10 °C min^{-1} to 900 °C with N_2 flow rate of 30 mL min^{-1}. Element analysis was carried out on a Germany Elementar large sample volume element analyzer, vario MACRO cube CHNS. PXRD data were collected on a PANalytical B.V. Empyrean powder diffractometer using a Cu Kα source (λ = 1.5418 Å) over the range of 2θ = 2.0−40.0° with a step size of 0.02° and 2 s per step. The sorption isotherm for N_2, CH_4 and CO_2 was measured by using a Quantachrome Autosorb-IQ analyzer with ultra-high-purity gas (99.999% purity). To estimate pore size distributions for PAE-COFs, nonlocal density functional theory (NLDFT) was applied to analyze the N_2 isotherm on the basis of the model of N_2@77 K on carbon with slit pores and the method of non-negative regularization. The SEM images were obtained on JEOL JSM6700 scanning electron microscope. The TEM images and EDS spectra were obtained on JEM-2100 transmission electron microscopy. The gas-separation property was tested by breakthrough experiments using a CO_2/CH_4/He or CO_2/N_2/He (25:25:50 v/v/v) gas mixture at a flow rate of 2.0 mL min^{-1} under room temperature. The relative amounts of the gases passing through the column were monitored on a Thermo Star gas analysis system detecting ion peaks at m/z+ 44 (CO_2), 16 (CH_4), 28 (N_2), 4(He).

Data availability. The authors declare that the data supporting the findings of this study are available within the Article and its Supplementary Information files, or from the corresponding author on reasonable request.

References

(1) Côté, A. P. *et al.* Porous, crystalline, covalent organic frameworks. *Science* **310,** 1166-1170 (2005).

(2) Colson, J. W. & Dichtel, W. R. Rationally synthesized two-dimensional polymers. *Nat. Chem.* **5,** 453-465 (2013).

(3) Huang, N., Wang, P. & Jiang, D. L. Covalent organic frameworks: a materials platform for structural and functional designs. *Nat. Rev. Mater.* **1,** 1-19 (2016).

(4) Diercks, C. S. & Yaghi, O. M. The atom, the molecule, and the covalent organic framework. *Science* **355,** 923-930 (2017).

(5) Ding, S. Y. & Wang, W. Covalent organic frameworks (COFs): from design to applications. *Chem. Soc. Rev.* **42,** 548-568 (2013).

(6) Jin, Y. H., Hu, Y. M. & Zhang, W. Tessellated multiporous two-dimensional covalent organic frameworks. *Nat. Rev. Chem.* **1,** 0056 (2017).

(7) Kuhn, P., Antonietti, M. & Thomas, A. Porous, covalent triazine-based frameworks prepared by ionothermal synthesis. *Angew. Chem. Int. Ed.* **47,** 3450-3453 (2008).

(8) Furukawa, H. & Yaghi, O. M. Storage of hydrogen, methane, and carbon dioxide in highly porous covalent organic frameworks for clean energy applications. *J. Am. Chem. Soc.* **131,** 8875-8883 (2009).

(9) Guan, X. Y. *et al.* Fast, ambient temperature and pressure ionothermal synthesis of three-dimensional covalent organic frameworks. *J. Am. Chem. Soc.* **140,** 4494-4498 (2018).

(10) Ding, S. Y. *et al.* Construction of covalent organic framework for catalysis: Pd/COF-LZU1 in suzuki miyaura coupling reaction. *J. Am. Chem. Soc.* **133,** 19816-19922 (2011).

(11) Fang, Q. R. *et al.* 3D microporous base-functionalized covalent organic frameworks for size-selective catalysis. *Angew. Chem., Int. Ed.* **53,** 2878-2882 (2014).

(12) Li, H. *et al.* 3D covalent organic frameworks with dual linkages for bifunctional cascade catalysis. *J. Am. Soc. Chem.* ***138,*** 14783-14788 (2016).

(13) Han, X. *et al.* Chiral covalent organic frameworks with high chemical stability for heterogeneous asymmetric catalysis. *J. Am. Chem. Soc.* **139,** 8693-8697 (2017).

(14) Wan, S., Guo, J., Kim, J., Ihee, H. & Jiang, D. L. A belt-shaped, blue luminescent, and semiconducting covalent organic framework. *Angew. Chem. Int. Ed.* **47,** 8826-8830 (2008).

(15) Bertrand, G. H. V., Michaelis, V. K., Ong, T. C., Griffin, R. G. & Dincă, M. Thiophene-based covalent organic frameworks. *Proc. Natl. Acad. Sci. USA* **110**, 4923-4928 (2013).

(16) Calik, M. *et al.* Extraction of photogenerated electrons and holes from a covalent organic framework integrated heterojunction. *J. Am. Chem. Soc.* **136**, 17802-17807 (2014).

(17) Fang, Q. R. *et al.* 3D porous crystalline polyimide covalent organic frameworks for drug delivery. *J. Am. Chem. Soc.* **137,** 8352-8355 (2015).

(18) Du, Y. *et al.* Ionic covalent organic frameworks with spiroborate linkage. *Angew. Chem. Int. Ed.* **55,** 1737-1741 (2016).

(19) Wang, S. *et al.* Exfoliation of covalent organic frameworks into few-layer redox-active nanosheets as cathode materials for lithium-ion batteries. *J. Am. Chem. Soc.* **139,** 4258-4261 (2017).

(20) Sun, Q. *et al.* Postsynthetically modified covalent organic frameworks for efficient and effective mercury removal. *J. Am. Chem. Soc.* **139,** 2786-2793 (2017).

(21) Li, Z. L. *et al.* Three-dimensional ionic covalent organic frameworks for rapid, reversible and selective ion exchange. *J. Am. Chem. Soc*. **139,** 17771-17774 (2017).

(22) Lu, Q. Y. *et al.* Postsynthetic functionalization of three-dimensional covalent organic framework for selective extraction of lanthanide ions. *Angew. Chem. Int. Ed.* **57,** 6042-6048 (2018).

(23) Kandambeth, S. *et al.* Self-templated chemically stable hollow spherical covalent organic framework. *Nat. Common.* **6,** 6786 (2015)**.**

(24) Mallick, A., Lukose, B., Mane, M. V., Heine, T. & Banerjee, R. Construction of crystalline 2D covalent organic frameworks with remarkable chemical (acid/base) stability via a combined reversible and irreversible route. *J. Am. Chem. Soc*. **134,** 19524-19527 (2012).

(25) Xu, H., Gao, J. & Jiang, D. L. Stable, crystalline, porous, covalent organic frameworks as a platform for chiral organocatalysts. *Nat. Chem.* **7,** 905-912 (2015).

(26) Wei, P. F. *et al.* Benzoxazole-linked ultrastable covalent organic frameworks for photocatalysis. *J. Am. Chem. Soc.* **140,** 4623-4631 (2018).

(27) Hergenrother, P. M. The use, design, synthesis, and properties of high performance/high temperature polymers: an overview. *High Performance Polymers* **15,** 3-45 (2003).

(28) Gao, Y. *et al.* Comparison of PEM properties of copoly(aryl ether ether nitrile)s containing sulfonic acid bonded to naphthalene in structurally different ways. *Macromolecules* **40,** 1512-1520 (2007).

(29) Gotham, K. & Turner, S. Poly(ether sulphone) as an engineering material. *Polymer* **15,** 665-670 (1974).

(30) McKeown, N. B. & Budd, P. M. Polymers of intrinsic microporosity (PIMs): organic materials for membrane separations, heterogeneous catalysis and hydrogen storage. *Chem. Soc. Rev*. **35,** 675-683 (2006).

(31) *Materials Studio ver. 7.0*, Accelrys Inc., San Diego, CA.

(32) Huang, N., Wang, P., Addicoat, M. A., Heine, T. & Jiang, D. L. Ionic covalent organic frameworks: design of a charged interface aligned on 1D channel walls and its unusual electrostatic functions. *Angew. Chem. Int. Ed.* **56,** 4982-4986 (2017).

(33) Du, N. *et al.* Polymer nanosieve membranes for CO_2-capture applications. *Nat. Mat.* **10,** 372-375 (2011).

(34) Henry, W. Experiments on the quantity of gases absorbed by water, at different temperatures, and under different pressures. *Philos. Trans. R. Soc. Lond.* **93,** 29-42 (1803).

(35) Fang, Q. R. *et al.* Designed synthesis of large-pore crystalline polyimide covalent organic frameworks. *Nat. Commun.* **5,** 4503 (2014).

(36) Guo J. *et al.* Conjugated organic framework with threedimensionally ordered stable structure and delocalized p clouds. *Nat. Commun.* **4,** 2736 (2013).

(37) Halder A. *et al.* Ultrastable Imine-based Covalent Organic Frameworks for Sulfuric Acid Recovery: An Effect of Interlayer Hydrogen Bonding. *Angew. Chem. Int. Ed.* **57,** 5797-5802 (2018).

(38) Katz, M. J. *et al.* A facile synthesis of UiO-66, UiO-67 and their derivatives. *Chem. Commun.* **49,** 9449-9451 (2013).

(39) Pan, Y. C., Liu, Y. Y., Zeng, G. F., Zhao, L. & Lai, Z. P. Rapid synthesis of zeolitic imidazolate framework-8 (ZIF-8) nanocrystalsin an aqueous system. *Chem. Commun.* 4**7,** 2071-2073 (2011).

(40) Stephen, S. Y., Samuel, M. F., Jonathan, P. H., Charmant, A. & Williams, I. D. A chemically functionalizable nanoporous material $[Cu_3(TMA)_2(H_2O)_3]_n$. *Science* **283,** 1148-1151 (1999).

(41) Eddaoudi, M. *et al.* Systematic design of pore size and functionality in isoreticular MOFs and their application in methane storage. *Science* **295,** 469-472 (2002).

(42) Du, N., Robertson, G. P., Song, J., Pinnau, I. & Guiver, M. D. High-performance carboxylated polymers of intrinsic microporosity (PIMs) with tunable gas transport properties. *Macromolecules* **42,** 6038−6043 (2009).

(43) Peng, C. *et al.* Diverse macroscopic helical motions of microribbons driven by electrons. *Chem. Comm.* **53,** 2578-2581 (2017).

(44) Sholl, D. S. & Lively, R. P. Seven chemical separations to change the world. *Nature* **533,** 316-322 (2016).

(45) Ali, I. New generation adsorbents for water treatment. *Chem. Rev.* **112,** 5073-5091 (2012).

(46) Wang, T. *et al.* Adsorptive removal of antibiotics from water using magnetic ion exchange resin. *J. Environ. Sci.* **52,** 111-117 (2017).

(47) Wang, Y., Pan, X., Wang, J., Hou, P. & Qiang, Z. J. Adsorption behavior and mechanisms of norfloxacin onto porous resins and carbon nanotube. *Chem. Eng. J.* **179,** 112-118 (2012).

(48) Ali, M. M. & Ahmed, M. J. Adsorption behavior of doxycycline antibiotic on NaY zeolite from wheat (Triticum aestivum) straws ash. *J. Institute Chem. Eng.* **81,** 218-224 (2017).

(49) Singh, S. *et al.* Nanocuboidal-shaped zirconium based metal organic framework for the enhanced adsorptive removal of nonsteroidal anti-inflammatory drug, ketorolac tromethamine, from aqueous phase. *New J. Chem.* **42,** 1921-1930 (2018).

(50) Hayashi, H., Aratani, N. & Yamada, H. Semiconducting self-assembled nanofibers prepared from photostable octafluorinated bisanthene derivatives. *Chem. Eur. J.* **23,** 7000-7008 (2017).

(51) Mason, C. R. *et al.* Polymer of intrinsic microporosity incorporating thioamide functionality: preparation and gas transport properties. *Macromolecules* **44,** 6471-6479 (2011).

(52) *Jade version 5.0,* Materials Data Inc., California.

Acknowledgements

Q.F., V.V., S.Q. and M.X. acknowledge the support of National Natural Science Foundation of China (21571079, 21621001, 21390394, 21571076 and 21571078), ″111″ project (B07016 and B17020), Guangdong and Zhuhai Science and Technology Department Project (2012D0501990028), and the program for JLU Science and Technology Innovative Research Team. Q.F and V.V. acknowledge the support from Thousand Talents program (China). V.V., Q.F., and S.Q. acknowledge the collaboration in the framework of China-French joint laboratory “Zeolites”.

Author contributions

Q.F., V.V., Y.Y. and S.Q. were responsible for the overall design, direction and supervision of the project. X.G. performed the experimental work. H.L. and Y.M. took SEM images and helped with the

TGA and PXRD tests. M.X. was in charge of other physical measurements. All authors discussed the results and contributed to the writing of the manuscript.

Additional information

Supplementary information is available in the online version of the paper. Reprints and permissions information is available online at www.nature.com/reprints. Correspondence and requests for materials should be addressed to Q.F., V.V., and Y.Y.

Competing financial interests

The authors declare no competing financial interests.

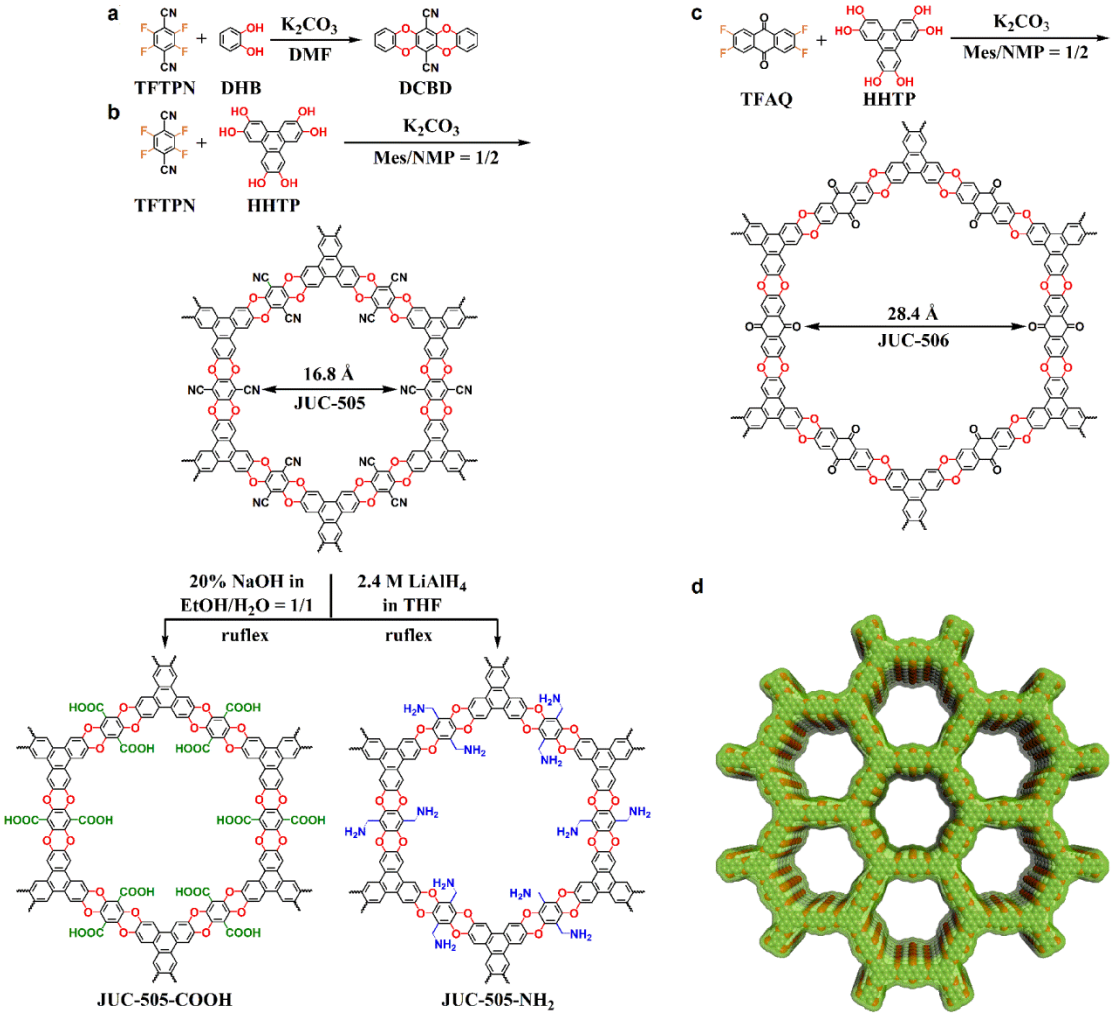


Figure 1 | Strategy for preparing stable porous crystalline PAE-COFs. a, The model reaction between TFTPN and DHB yields a dioxin product, DCBD. **b,** Condensation of TFTPN and HHTP gives a 2D microporous crystalline PAE-COF with pore size of 16.8 Å, denoted JUC-505. The functionalized PAE-COFs, JUC-505-COOH and JUC-505-NH_2, can be obtained after the post-modification of JUC-505. **c,** TFAQ and HHTP forms a 2D mesoporous crystalline PAE-COF with pore size of 28.4 Å, denoted JUC-506. **d,** Condensation of linear and triangular building units constructs a 2D porous structure based on the boron nitride net (**bnn**).

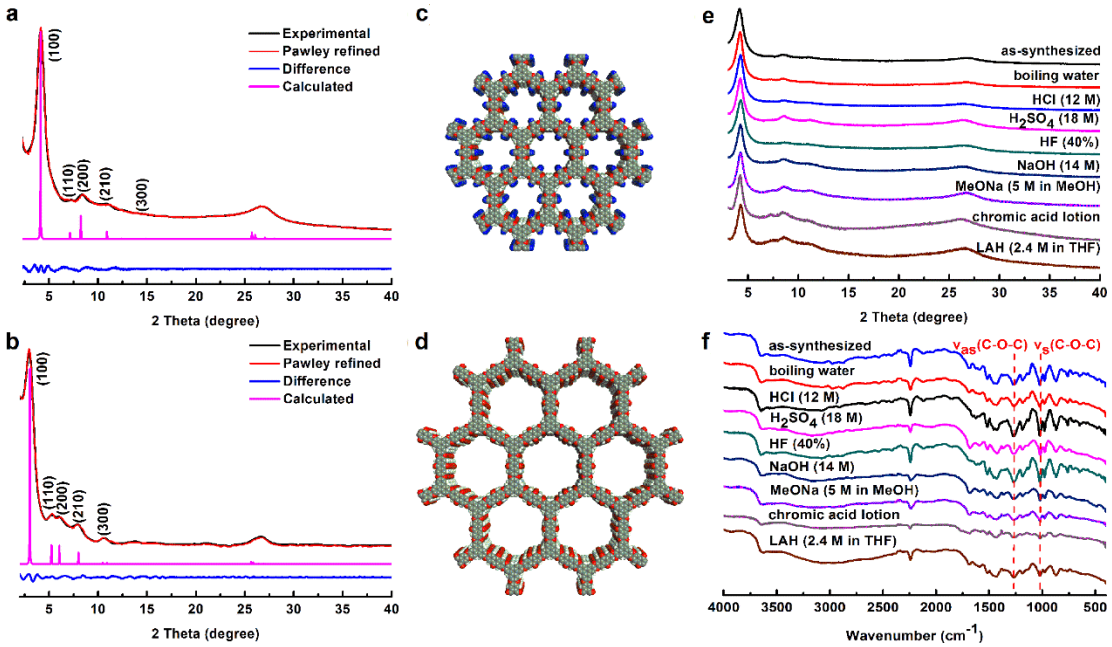


Figure 2 | Crystallinity and stability. a and b, PXRD profiles of JUC-505 and JUC-506, respectively. Experimentally observed (black), Pawley refined (red), their difference (blue) and calculated using the AA stacking mode (magenta). **c and d,** Structure representation of the AA stacking mode of JUC-505 and JUC-506, respectively (O, red; N, blue; C, grey; H, white). **e and f,** PXRD patterns and IR spectra of JUC-505 after treatments under different chemical environments for one week.

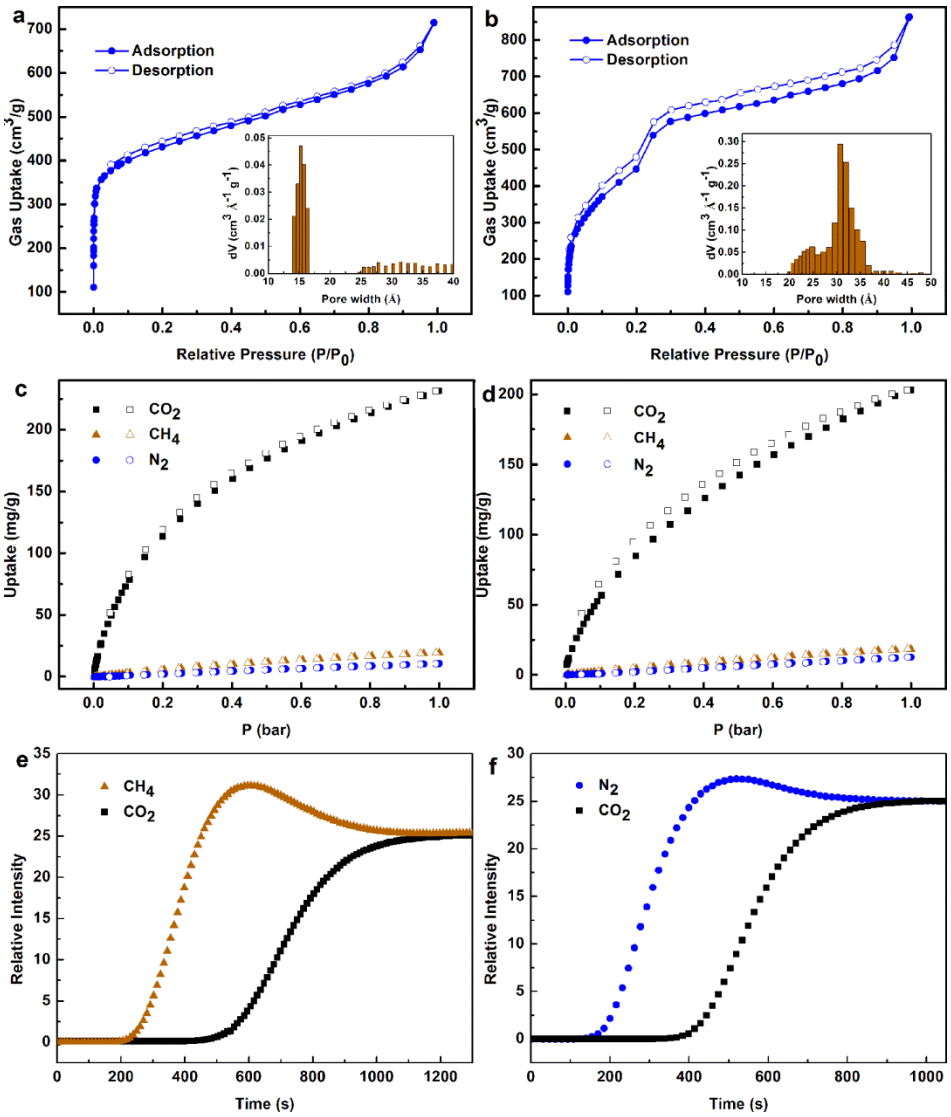


Figure 3 | Gas adsorption and separation. a and b, N_2 adsorption-desorption isotherms at 77 K for JUC-505 and JUC-506, respectively. Inset: pore size distributions from fitting the NLDFT model to the adsorption data. **c and d,** CO_2 separation properties over CH_4 and N_2 at 273 K for JUC-505 and JUC-506, respectively. **e and f,** Breakthrough curves for JUC-505 using the CO_2/CH_4 and CO_2/N_2 gas mixture.

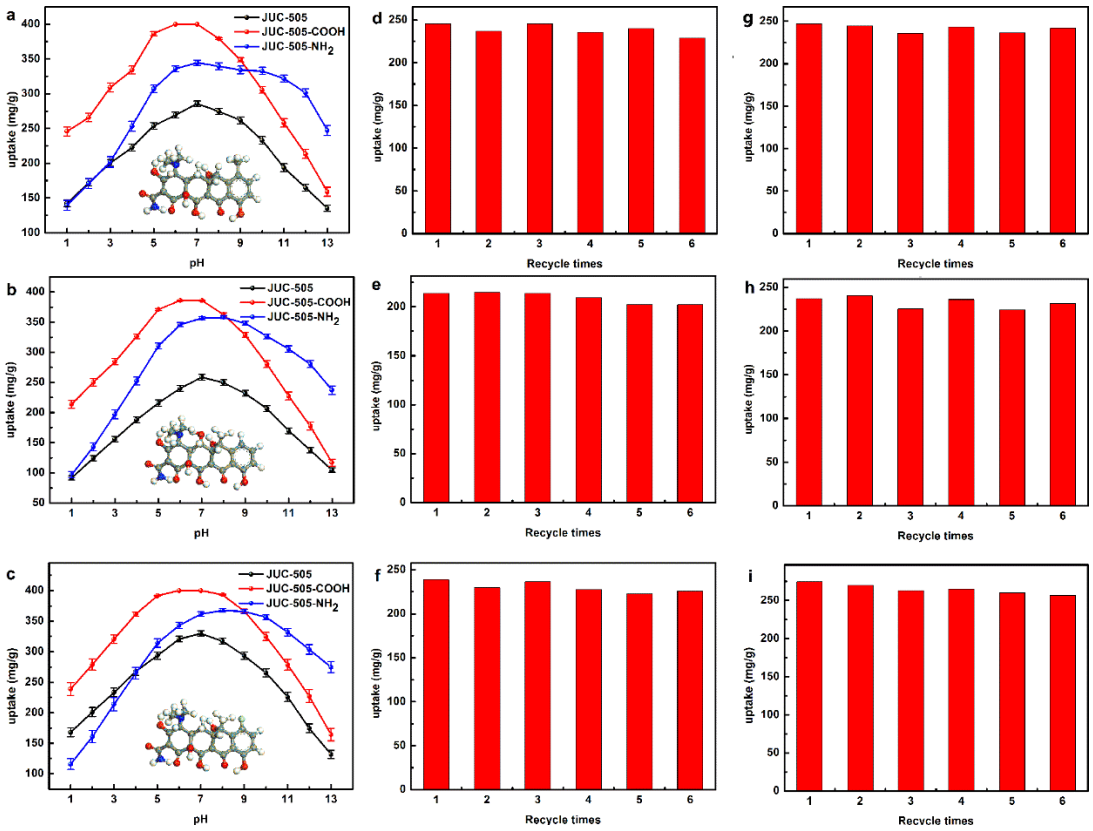


Figure 4 | Study of antibiotic uptakes. a-c, TCN, OTC and CTC uptakes at different pH (initial concentration = 200 mg/L, contact time = 72 h, sorbent dosage = 0.5 g/L, temperature = 298 K). Inset: molecular structure of TCN, OTC and CTC. O, red; N, blue; C, grey; H, white; Cl, cyan. **d-f,** Recycling test of TCN, OTC and CTC uptakes of JUC-505-COOH at pH = 1. **g-i,** Recycling test of TCN, OTC and CTC uptakes of JUC-505-NH_2 at pH = 13.

Table 1 | Experimental and modelling results of gas adsorption on PAE-COFs.

PAE -COFs	BET	Pore volume	LPD[a]	Temperature	Uptake mg g^{-1}			Ideal adsorption selectivity[b]	
	$m^2 g^{-1}$	$cm^3 g^{-1}$	Å	K	CO_2	CH_4	N_2	CO_2/CH_4	CO_2/N_2
JUC-505	1584	0.51	16.8	273	231.3	19.2	10.4	48.9	97.2
				298	189.0	15.2	8. 8	33.8	65.6
JUC-506	1655	0.71	28.4	273	203.0	18.3	12. 5	33.5	69.0
				298	159.2	13.1	8. 9	24.2	44.1

[a]Largest pore diameter (LPD) obtained theoretically; [b]Calculated using the initial slope in the Henry region of isotherms at 273 K and 298 K based on Henry's law.

Table 2 | Stability after the treatment under various chemical environments for one week.[a]

CPMs		Boiling water	HCl	H_2SO_4	HF	NaOH	MeONa	$LiAlH_4$	Chromic acid
COFs	JUC-505	√	√	√	√	√	√	√	√
	JUC-506	√	√	√	√	√	√	√	√
	DhaTab-COF[23]	√	×	×	×	×	×	√	×
	TpPa-1[24]	√	√	×	×	×	×	√	×
	TPB-DMTP-COF[25]	√	×	×	×	√	√	×	×
	LZU-190[26]	√	×	×	√	×	×	√	×
	PI-COF-2[35]	√	×	×	×	×	×	√	×
	CS-COF[36]	√	√	×	×	×	×	√	×
	TpOMe-Pa1[37]	√	√	×	×	×	×	√	×
MOFs	UiO-66[38]	×	×	×	×	×	×	×	×
	ZIF-8[39]	×	×	×	×	×	×	×	×
	HKUST-1[40]	×	×	×	×	×	×	×	×
	MOF-5[41]	×	×	×	×	×	×	×	×
Zeolites	Silicalite-1[b]	×	×	×	×	×	×	×	×
	X[b]	×	×	×	×	×	×	×	×
	Y[b]	×	×	×	×	×	×	×	×
	4A[b]	×	×	×	×	×	×	×	×

[a]The stabilities of the samples were determined by PXRD patterns. Green with the tick represents stable, and red with the cross represents unstable.

[b]The chemicals were obtained from commercial sources.